

## Effects of sulphur doping on properties of CoO for various applications: a DFT+U study.

Henry S. Ezeaku<sup>1</sup>, Anthony N. Eze<sup>1</sup>, Victor C Asamonye<sup>1</sup>, Abdulrafiu T. Raji<sup>2</sup>, Timothy C. Chibueze<sup>3,4</sup>

<sup>1</sup> Department of Metallurgical and Materials Engineering, University of Nigeria, Nsukka 410001 Nigeria

<sup>2</sup> Center for Augmented Intelligence and Data Science (CAIDS), College of Science, Engineering and Technology (CSET), University of South Africa (UNISA), PO Box 392, Pretoria 0003, South Africa

<sup>3</sup> Department of Physics and Astronomy, University of Nigeria, Nsukka, 410001 Nigeria

<sup>4</sup> Africa Centre of Excellence for Sustainable Power and Energy Development (ACE-SPED), University of Nigeria, Nsukka

### ARTICLE INFO

#### Article history:

Received xxxxx

Revised xxxxx

Accepted xxxxx

Available online xxxxx

#### Keywords:

Sulphur-doped  
CoO,  
DFT+U,  
Electronic  
structure,  
Optical properties  
Antiferromagnetism

### ABSTRACT

Transition metal oxides have been tipped for versatile applications owing to the flexibility of their properties based on doping and prevailing experimental conditions. In this study, the electronic, optical, and magnetic properties of sulphur-doped cobalt oxide,  $\text{CoO}_{1-x}\text{S}_x$  ( $x = 0.125, 0.25, 0.375,$  and  $0.5$ ) was studied using density functional theory (DFT) and its Hubbard  $U$  modified variant (DFT+ $U$ ). Electronic structure analysis showed notable changes in the electronic energy structure as the dopant concentration increases. Our result showed that the significant effect of doping CoO with sulphur is the lowering of the electronic energy gap to a size which enhances absorption in the visible regime of the solar energy for efficient photovoltaic and other applications. Investigation of the magnetic properties showed that  $\text{CoO}_{1-x}\text{S}_x$  exists in antiferromagnetic ground state. Our studies provide useful insights into the mechanism for enhancing the performance of CoO through non-metal doping for photovoltaic and other applications.

### 1. Introduction

Transition metal oxides and chalcogenides hold significance in contemporary material science [1] due to their fascinating properties [2], [3], [4] and among these are the cobalt (Co) based oxides [5]. In particular, cobalt (ii) oxide (CoO) has been proposed for applications in solar cell, water splitting, supercapacitor and battery [6]. Experimental and computational investigations indicate that CoO exists in cubic as well as wurtzite structure depending in the experimental conditions.

\*Corresponding author: Timothy C. Chibueze

E-mail address: [timothy.chibueze@unn.edu.ng](mailto:timothy.chibueze@unn.edu.ng)

<https://doi.org/10.60787/tnamp.v20.379>

1115-1307 © 2024 TNAMP. All rights reserved

It has been known as one of the few transition metal-oxide nanocrystals that display unconventional physical properties that are absent in most bulk materials [7], [8], and exhibits antiferromagnetic (AFM) semiconducting properties [9]. Computational material research has garnered significant interest for its role in predicting and interpreting the correlations between the band structures of materials and their relevant properties [10]. Pure CoO, with a electronic energy gap between 2.0 eV to 3.0 eV, demonstrates limited absorption of visible light and primarily becomes energized only when exposed to ultraviolet light [11]. With a Néel temperature close to that of room temperature [12], CoO also possesses a wurtzite structure, placing it among transition metal-oxide nanocrystals known for displaying unconventional physical properties that are absent in most bulk materials [7], [8]. In nanomaterials, doping plays a crucial role in stabilizing a particular crystallographic phase and altering its properties [13]. Many research groups have studied the effect of doping CoO with various metal elements on its properties. For example, Yin and his group [14] applied first principles calculations to study Zn and Ti doped CoO. Their result revealed that CoO with antiferromagnetic ground state was transformed into ferromagnetic state by Zn doping while Ti doping transformed it from semiconductor to metal thereby enhancing its conductivity. Also, Liu et al [15] in their first principles studies revealed that 3.125% and 2.083% La doped CoO exhibited half-metallic properties. According to another first-principles study by Liu [16] on transition metal-doped CoO, Cr and Fe-doped structure exhibited half-metallic behavior with high spin polarization, crucial for spintronic device design. In a similar endeavour, Cu-doped CoO nanorods, exhibited enhanced performance as lithium-ion battery anodes [17]. Another group studied Ni doped CoO. The outcome of the study showed that Ni doped CoO nanosheets enhanced oxygen reduction reaction activity, leading to outstanding power density of  $377 \text{ mW cm}^{-2}$  at discharge peak, stability of over 400 hours at  $5 \text{ mA cm}^{-2}$ , as well as a rechargeable battery operating at charge-discharge voltage as little as 0.63 V, surpassing Pt/C catalyst-based devices [18]. These results show that doping could alter the properties of CoO in fascinating and useful ways making it relevant for multiple applications.

However, there are few literature on non-metal doped CoO. Non-metal doping of CoO and in particular sulphur doping could expose further fascinating properties for photovoltaic and other applications. This study therefore focuses on the structural, electronic, optical and magnetic properties of the cubic CoO doped with sulphur at different concentrations using density functional theory for various applications. Our study also investigated the effect of incorporating onsite Coulomb interaction,  $U$  to DFT (DFT+ $U$ ) on the electronic properties. Section 1 contains the introduction; section 2 is the computational details while our results and conclusions are respectively presented in sections 3 and 4.

## 2. Calculation Models and Methods

In our studies, zinc blende structure was adopted for the pristine CoO. We used  $2 \times 2 \times 2$  primitive unit cell of CoO to study the effect of sulphur dopant on CoO. Various concentrations of sulphur were considered for  $\text{CoO}_{1-x}\text{S}_x$ ; the concentration  $x$  is 0.125, 0.25, 0.375, and 0.5 corresponding to 12.5%, 25% and 37.5% and 50% sulphur concentrations. For each doped structure, some oxygen atoms are substituted with sulphur atoms and the structure is fully relaxed. The doped structures were created using the Monte Carlo simulation for quasi random structures embedded in the alloy theoretic atomistic toolkit [19]. We used first principles DFT [20] within the Kohn-Sham [21] approach in our calculations with planewaves basis set as implemented in the quantum espresso code (QE) [22]. Exchange correlation functional was estimated using the Perdew, Burke and Ernzerhof (PBE) [16] parameterization. The interaction of the ionic cores with the valence electrons were defined using norm-conserving pseudopotentials [23] with valence electron configurations of  $4s^2 3d^7$  for Co,  $2s^2 2p^4$  for O, and  $3s^2 3p^4$  for S. The expansion of the

wavefunction was done with cutoff energy of 80 Ry. For sampling the irreducible Brillouin zone,  $16 \times 16 \times 16$  and  $8 \times 8 \times 8$  [24] Monkhorst-Pack grid was used for primitive unit cell and the supercell respectively. The self-consistent iteration convergence threshold was established at  $10^{-4}$  Ry/atom. Complete relaxation of lattice constants and atomic positions in each supercell was performed until each atom experienced a maximal force of less than 0.003 Ry/Bohr. To address the band gap limitation of GGA, we implemented DFT+U which corrects the on-site Coulomb interaction [25] using the Dudarev approach [26]. The value of 5.7347 eV we used for the effective U parameter ( $U_{\text{eff}}$ ) was calculated following the self-consistent approach developed by Timrov et al [27], [28]. The optical properties were calculated within the DFT+U calculations using the epsilon.x module in the Quantum ESPRESSO (QE) code. The optimized parameters were used in the optical calculations.

### 3. Results

#### 3.1 Structural properties

The structure of the pristine and sulphur doped CoO with compositions of 0, 0.125, 0.25, 0.375, and 0.5 (see Figure 1) were optimized using the standard DFT and the calculated lattice parameters are presented in Table 1.

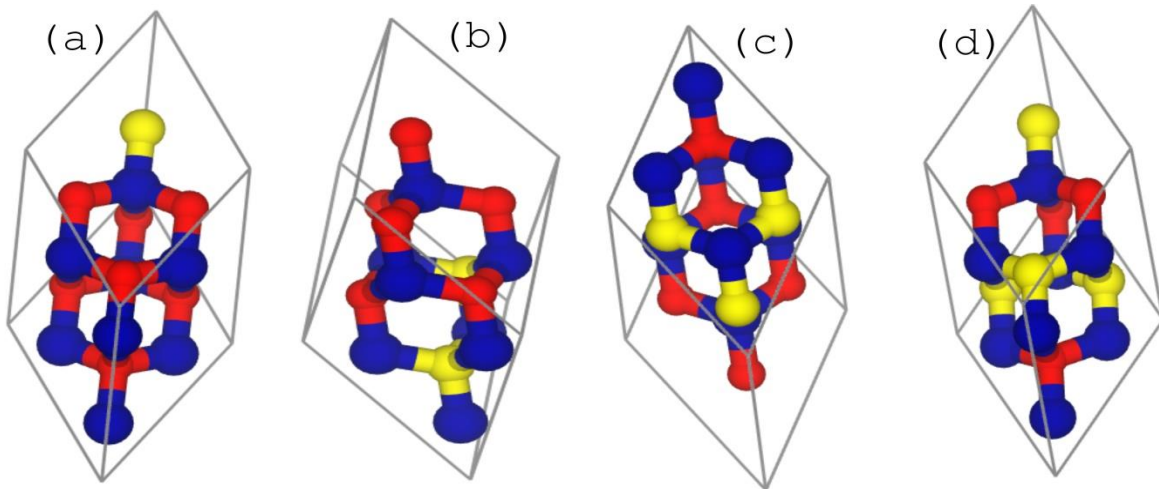


Figure 1: Crystal structure of  $\text{CoO}_{1-x}\text{S}_x$  for sulphur concentrations, (a)  $x = 0.125$  (b)  $x = 0.25$  (c)  $x = 0.375$  and (d)  $x = 0.5$  created using the  $2 \times 2 \times 2$  primitive unit cell of the cubic CoO. Co, O, and S are denoted by blue, red, and yellow spheres respectively.

Table 1: Lattice constants  $a$  ( $\text{\AA}$ ) and electronic energy gap (eV) of pristine and doped CoO at sulphur concentration  $x = 0.125, 0.25, 0.375,$  and  $0.5$ . The lattice constant and band gap was calculated using GGA and GGA+U respectively.

$x$	0	0.125	0.25	0.375	0.5
$a$ ( $\text{\AA}$ )	4.27	4.31	4.23	4.29	4.49
	4.25 <sup>a</sup> 4.31 <sup>b</sup>				
Band Gap (eV)	0.34 <sup>+</sup> 1.63 2.6 <sup>c</sup>	0.22 <sup>+</sup> 1.65	0.43	0.63	0.53

<sup>a</sup>Ref. [29], <sup>b</sup>Ref. [30], <sup>c</sup>Ref. [31], <sup>+</sup> signifies band gap calculated using GGA.

Our result showed that the lattice constants of the CoO varied with sulphur concentration. Normally, since the atomic radius of sulphur is greater than that of oxygen, an increase in the lattice constants as sulphur concentration increases is expected. Our result shows an increase in lattice constant at doping concentration of 0.125 and 0.5. However, the lattice constant decreases at doping concentration of 0.25 and 0.375. The lattice constant at doping concentration of 0.25 is even lower than that of the pristine CoO. These decrease in lattice constant doping concentration of 0.25 and 0.375 could be attributed to strong hybridization between oxygen and sulphur at these concentrations leading to higher mass density and mechanical stability of the structures. This may also influence the material's catalytic activity and ion diffusion properties, crucial for applications in energy storage and conversion at these concentrations. Also, from Table 1, there is a fair agreement between our GGA calculated lattice constant gotten for the pristine CoO, with other data from experiments and other theoretical methods. The band gap values for the pristine CoO and  $\text{CoO}_{1-x}\text{S}_x$  ( $x=0.125, 0.25, 0.375,$  and  $0.5$ ) are also displayed in Table 1.

### 3.2 Electronic properties

Figures 2 to 6, show the calculated electronic band structure and atom projected density of states (PDOS) for optimized pristine CoO and  $\text{CoO}_{1-x}\text{S}_x$  ( $x=0.125, 0.25, 0.375,$  and  $0.5$ ). The electronic properties and PDOS computed for the undoped CoO and shown in Figure 2(a) using standard GGA reveal that cubic CoO is a direct band gap semiconductor with 0.34 eV energy gap at the  $\Gamma$ -point. Due to the low band gap value given by DFT as a result of well-known intrinsic factor of DFT, more accurate energy gap of 1.63 eV at the  $\Gamma$ -point was estimated using GGA+U and presented in Figure 2(b). The PDOS in Figures 2(a) and 2(b) show that the lower energy portion of the valence band comes largely from Co-3d spin-down orbitals while the upper valence band are mainly from Co-3d spin-up states. The dominant contributors to the lower conduction band are the Co-3d spin-up with minor contribution from O-2p orbitals. In order to examine the impact of sulphur doping on the electronic properties of CoO, we calculated the band structure, and density of states (DOS) by substituting one sulphur site with an oxygen atom, corresponding to doping concentration  $x = 0.125$ , as illustrated in Figure 3 for GGA and GGA+U. The main effect of S-doping at concentration of 0.125 on the electronic structure (see Figure 3) is to reduce (increase) the size of the energy gap to 0.22 eV (1.65 eV) using GGA (GGA+U). The valence band is composed of hybridization of Co-3d spin-down, O-2p, and S-2p states with the top of the valence band dominated by the Co-3d spin-down states. Also, the dominant contributors to the lower part of the conduction band are the Co 3d spin-up and O 2p states. For doping concentration of 0.25 (see Figure 4), GGA shows metallic character without band gap indicating a transition from semiconductor to metallic behaviour. However, GGA+U presented in Figure 4(b) showed a direct energy gap  $\sim 0.43$  eV at the  $\Gamma$ -point. The band gap at  $x=0.25$  is much lower than that of the pristine CoO (1.63eV) and that at  $x=0.125$ . The upper valence band constitutes mainly of the O-2p while the lower valence band is dominated by the Co-3d spin-up with little contribution by the S-2p. The major contributor of the conduction band is the Co-3d spin-down states. The result for dopant concentration of 0.375 and 0.5 are presented in Figures 5 and 6 respectively. Both dopant concentration of 0.375 and 0.5 shows the absence of band gap for the GGA calculation (Figures 5 and 6 respectively) suggesting a trend toward metallic behaviour. However, GGA+U result shown in Figures 5b and 6b for dopant concentration of 0.375 and 0.5 respectively displayed a direct band gap at point  $\Gamma$  with energy gap  $\sim 0.63$  eV and 0.53 eV respectively. The major constituent of the upper valence band is O-2p while the lower valence band are Co-3d spin-up and S-2p. The main contributor to the conduction band for the 0.375 doping concentrations is the Co-3d spin-down states. In the compound with doping concentration of 0.5, O-2p states is dominant in the valence band while Co-3d spin-up is dominant in the lower part of the conduction band.

Our results on the electronic properties show that the significant effect of the S-doping on the properties of CoO is to reduce the size of the energy gap. This is observed in Figures 2-6(a) calculated at the standard GGA level of the theory where the doping concentration of 0, 0.125 and 0.25 are 0.34 eV, 0.22 eV and 0 eV respectively. This implies that GGA predicts that the cubic CoO becomes a metal at sulphur doping concentration of 0.25 and above. However, using the GGA+U, the energy gap at doping concentrations of 0.125 and 0.25 does not follow the sequential decreasing order of the energy band gap. Doping concentration of 0.125 shows energy band gap  $\sim 1.65$  eV which is above that of the pristine ( $\sim 1.63$  eV). Also, the band gap of doping concentration of 0.25 is less than the band gaps at doping concentrations of 0.375 and 0.5. This suggests that the exceptional strong hybridization between the Co-3p, O-2p and S-2p orbitals at these doping concentrations which might be responsible for this deviation for the energy gap trend.

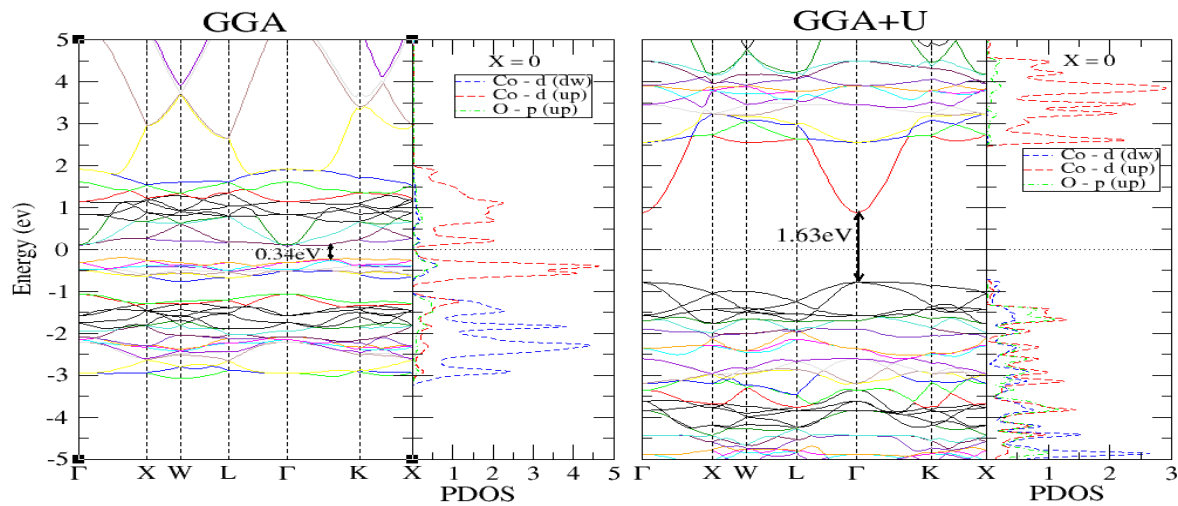


Figure 2: Energy band structure and density of states projected at the atomic orbitals (PDOS) of  $\text{CoO}_{1-x}\text{S}_x$  ( $x = 0$ ) using (a) standard GGA and (b) GGA+U

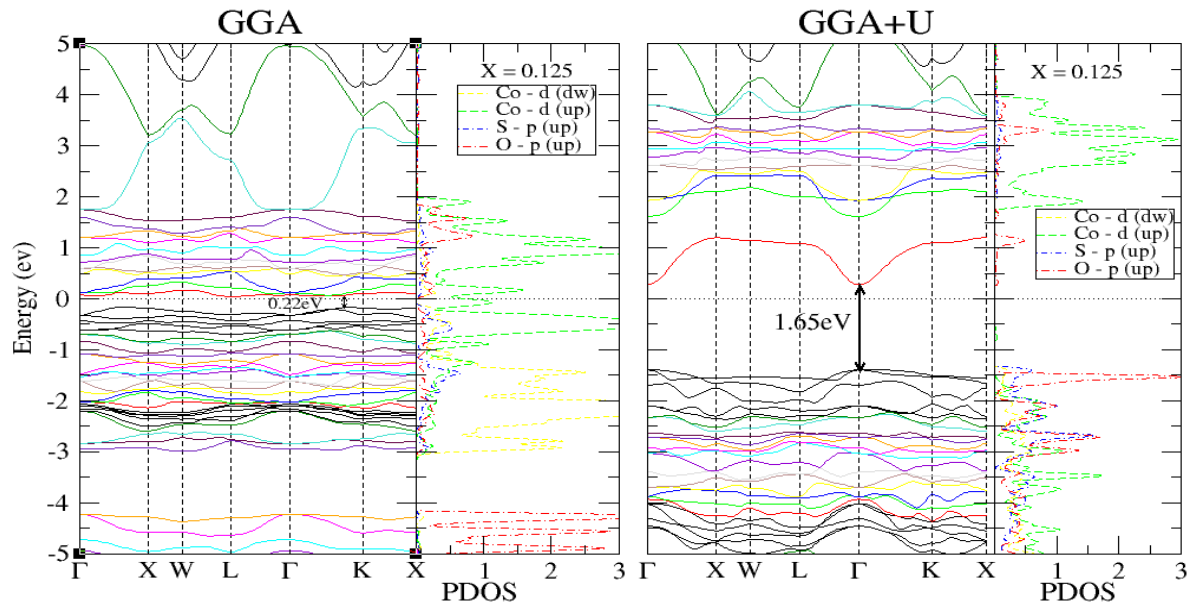


Figure 3: Energy band structure and density of states projected at the atomic orbitals (PDOS) of  $\text{CoO}_{1-x}\text{S}_x$  ( $x = 0.125$ ) using (a) standard GGA and (b) GGA+U

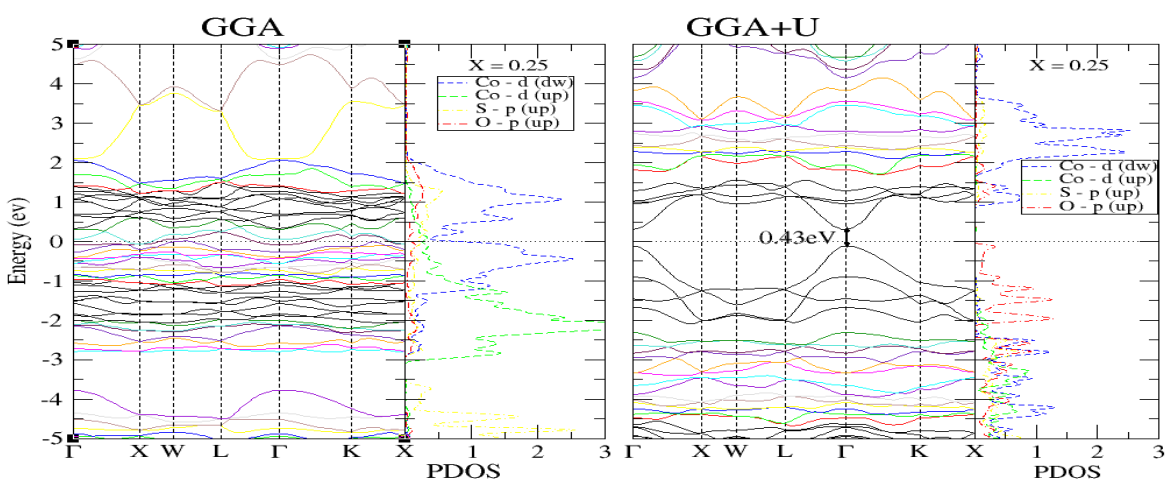


Figure 4: Energy band structure and density of states projected at the atomic orbitals (PDOS) of  $\text{CoO}_{1-x}\text{S}_x$  ( $x = 0.25$ ) using (a) standard GGA and (b) GGA+U

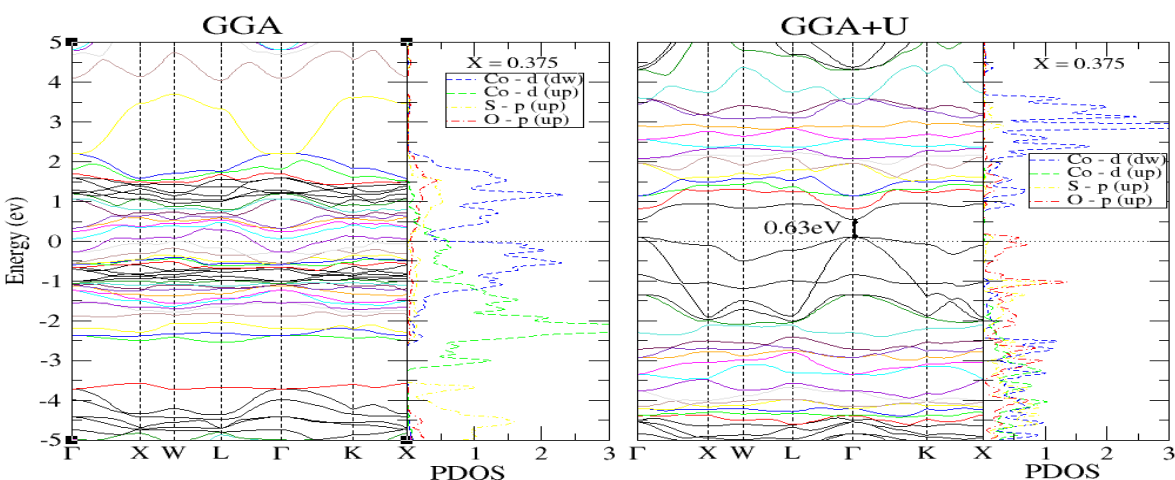


Figure 5: Energy band structure and density of states projected at the atomic orbitals (PDOS) of  $\text{CoO}_{1-x}\text{S}_x$  ( $x = 0.375$ ) using (a) standard GGA and (b) GGA+U

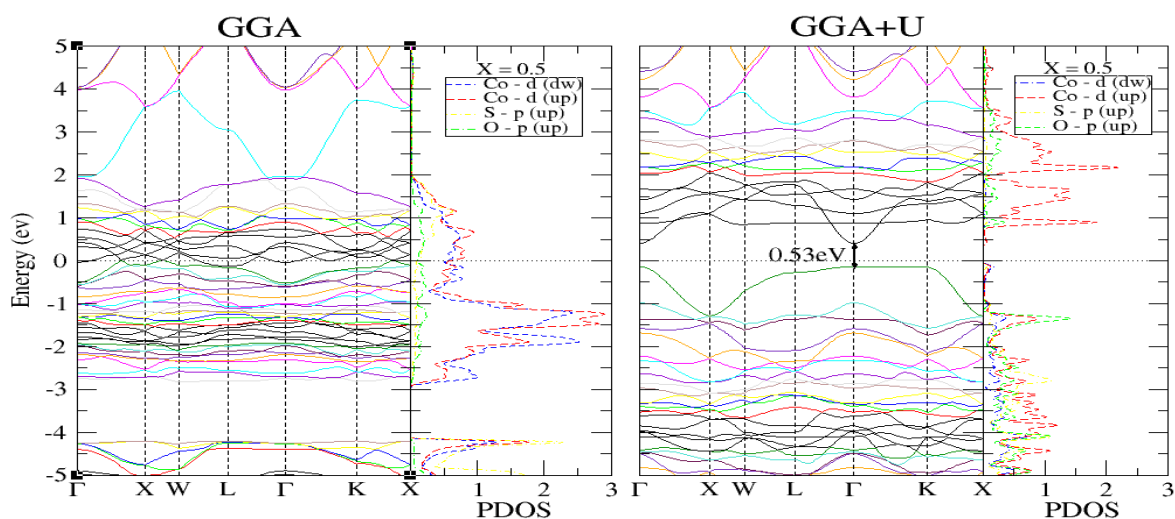


Figure 6: Energy band structure and density of states projected at the atomic orbitals (PDOS) of  $\text{CoO}_{1-x}\text{S}_x$  ( $x = 0.5$ ) using (a) standard GGA and (b) GGA+U

### 3.3 Optical Property

To understand the optical absorption spectra of the S doped compounds and pure CoO, the dielectric function  $\epsilon(\omega)$  was computed to find the real ( $\epsilon_1$ ) and imaginary ( $\epsilon_2$ ) parts (see equation 1) using epsilon.x in QE code [33] at the GGA+U level of theory. Optical absorptions in materials are basically determined by the transition matrix elements between the valence and conduction band orbitals, as well as their density of states (DOS) [34]

$$\epsilon(\omega) = \epsilon_1(\omega) + \epsilon_2(\omega) \quad 1$$

Using the real and imaginary components of the dielectric function, the optical absorption spectra  $\alpha(\omega)$ , refractive index  $n(\omega)$ , and reflectivity  $R(\omega)$  were also computed [35]:

$$\alpha(\omega) = \frac{\omega \epsilon_2(\omega)}{c} \quad 2$$

$$n(\omega) = \frac{1}{\sqrt{2}} [(\epsilon_1^2(\omega) + \epsilon_2^2(\omega))^{1/2} + \epsilon_1(\omega)]^{1/2} \quad 3$$

$$R(\omega) = \frac{(n-1)^2 + \epsilon_2^2}{(n+1)^2 + \epsilon_2^2} \quad 4$$

Figure 7(a) shows the relationship between the dielectric function and photon energy (eV) for the pristine CoO. Using the plot of the optical characteristics shown in Figure 7(a), the imaginary part of the dielectric function ( $\epsilon_2(\omega)$ ), it is seen that there are three major peaks corresponding to the energy levels of 1.75eV, 4.19eV, and 7.94eV. The transition between the Co-3d spin-up and O-2p states in the valence band is responsible for the peak at 1.75 eV; the transition between the Co-3d spin-down and O-2p states is responsible for the peak at 4.19 eV; and the transition between the O-2p and the Co-3d states (not shown) is responsible for the peak at 7.94 eV. Figure 8(a) shows the dependence of dielectric function on energy for  $\text{CoO}_{1-x}\text{S}_x$  ( $x = 0.125, 0.25, 0.375$  and  $0.5$ ). At  $x = 0.125$ , the imaginary part of the dielectric constant has two major peaks at 1.76 eV and 5.25 eV. The 1.76 eV peak results from a transition between the O-2p in the upper part of the valence band and the Co-3d spin-up state in the conduction band, while the 5.25 eV peak results from a transition between the Co-3d spin-down and the Co-3d spin-up states in the valence band.. For  $x = 0.25$ , the major peaks are 2.65 eV and 5.09 eV; the major peaks for  $x = 0.375$  are at 0.45 eV and 4.84 eV; the major peaks for  $x = 0.5$  are at 1.43 eV and 3.22 eV. The transition between Co-3d spin-down and O-2p, S-2p and O-2p, and Co-3d spin-up and O-2p, respectively, is responsible for the peak at 2.65 eV, 0.45 eV, and 1.43 eV. On the other hand, the peak at 5.09eV, 4.84eV and 3.22eV are caused by the transition between the Co-3d spin-down and S-2p, Co-3d spin-up and Co-3d spin-down, S-2p and Co-3d spin-up, respectively.

Figures 7(b) and 8(b) shows the absorption spectra for the pristine CoO and that with various sulphur concentrations, respectively. The amount of light of a given wavelength that can enter a material before being absorbed is determined by its absorption coefficient. One of the most important factors affecting a material's photo-catalytic activity is its capacity to absorb light. From Figure 7(b), CoO showed majorly high absorption spectra within the ultraviolet region; but, showed no absorption spectra within the visible light and infra-red region. This is because, CoO typically has a bandgap in the ultraviolet (UV) range, indicating that it requires higher-energy photons to induce electronic transitions and since the bandgap is beyond the visible light range, it will not efficiently absorb visible light, leading to the lack of absorption peaks in that region. On the other hand, Figure 8(b)'s absorption spectra for the sulphur-doped CoO show a strong absorption peak in the ultraviolet area, a small peak in the visible light region, and no peaks in the infrared. The addition of sulfur has altered the electronic band structure of CoO, resulting in a

decrease in the band gap and the formation of a peak in the visible light area. This makes CoO more viable for absorption of visible light. From Figure 8(b), within the visible light region, the absorption peak intensity increases with an increase in sulphur concentration. Where, the 0.125 at% has the lowest absorption intensity within the visible region and the 0.5 at% has the highest. Since the doped CoO demonstrates enhanced absorption in the visible range, it will be useful for solar cells and also in improving photo-catalytic activity as compared to pure CoO.

Comparing the various peaks in Figures 7(b) and 8(b), the most prominent peak intensity for pristine CoO is  $4.29 \times 10^{27} \text{ cm}^{-1}$ , while that for the doped CoO are:  $3.62 \times 10^{27} \text{ cm}^{-1}$ ,  $3.56 \times 10^{27} \text{ cm}^{-1}$ ,  $3.41 \times 10^{27} \text{ cm}^{-1}$ , and  $3.55 \times 10^{27} \text{ cm}^{-1}$ , for  $x = 0.125, 0.25, 0.375,$  and  $0.5$  respectively. As the concentration of sulfur increases, Figure 8(b) shows that the energy of the absorption peaks somewhat lowers, with a little rise in deviation at concentrations of 0.5. This might be due to the fact that doping with sulphur might have altered the electronic band structure of CoO by narrowing the band gap. Hence, as the concentration of sulphur increases, the bandgap decreases, leading to a decrease in energy of the absorption peaks.

The refractive index and reflectivity of the pristine and the doped CoO shown in Figures 9 and 10, respectively are obtained using equations 3 and 4 above. The refractive index quantifies how a light ray changes direction when transitioning from one medium to another. From Figure 9, within the visible light region, the refractive index increases with increase in sulphur concentration with reference to the pristine CoO. Also, Figure 10 shows that addition of sulphur increases the reflectivity compared to the CoO. Reflectivity as a measure of the reflective quality or power of a surface or material is important in efficiency of a material for solar cell application. When sulfur content rises from 0.125 to 0.5 eV, reflectivity increases from 2.04 eV to 14.2 eV.

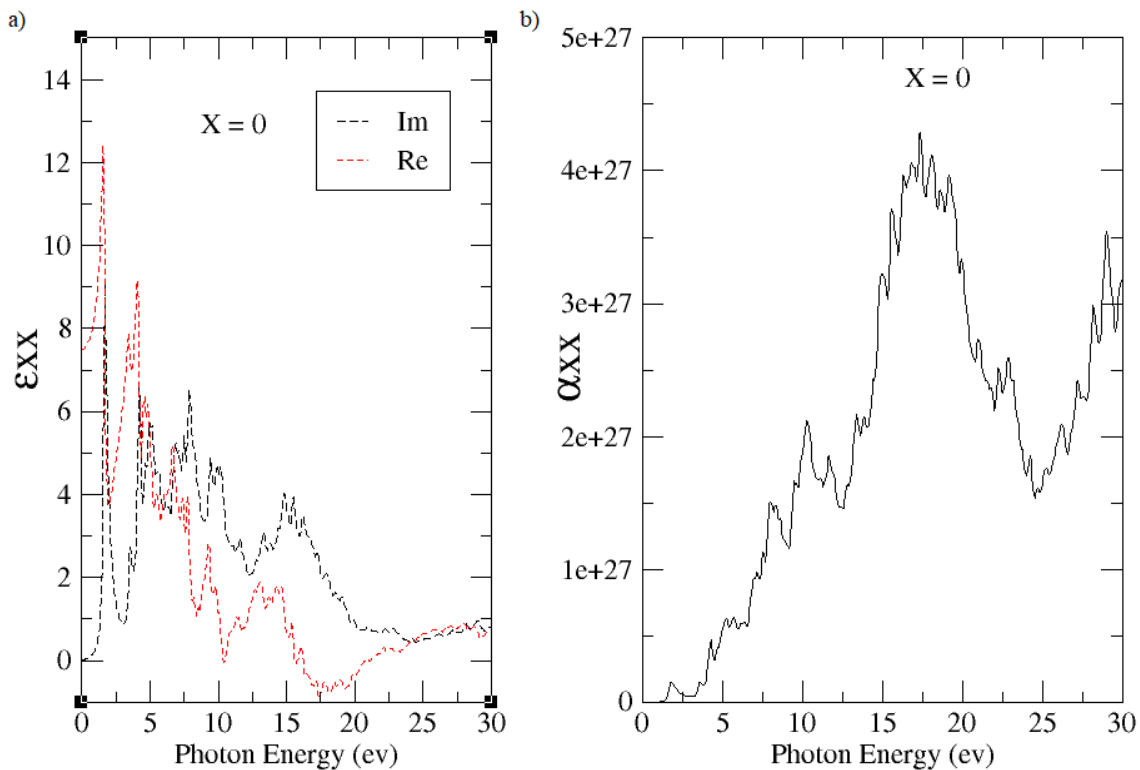


Figure 7: (a) Real and imaginary part of the dielectric function for the pristine  $\text{CoO}_{1-x}\text{S}_x$  at  $x = 0$  (b) absorption coefficient spectrum of the pristine  $\text{CoO}$   $\text{CoO}_{1-x}\text{S}_x$  at  $x = 0$ .

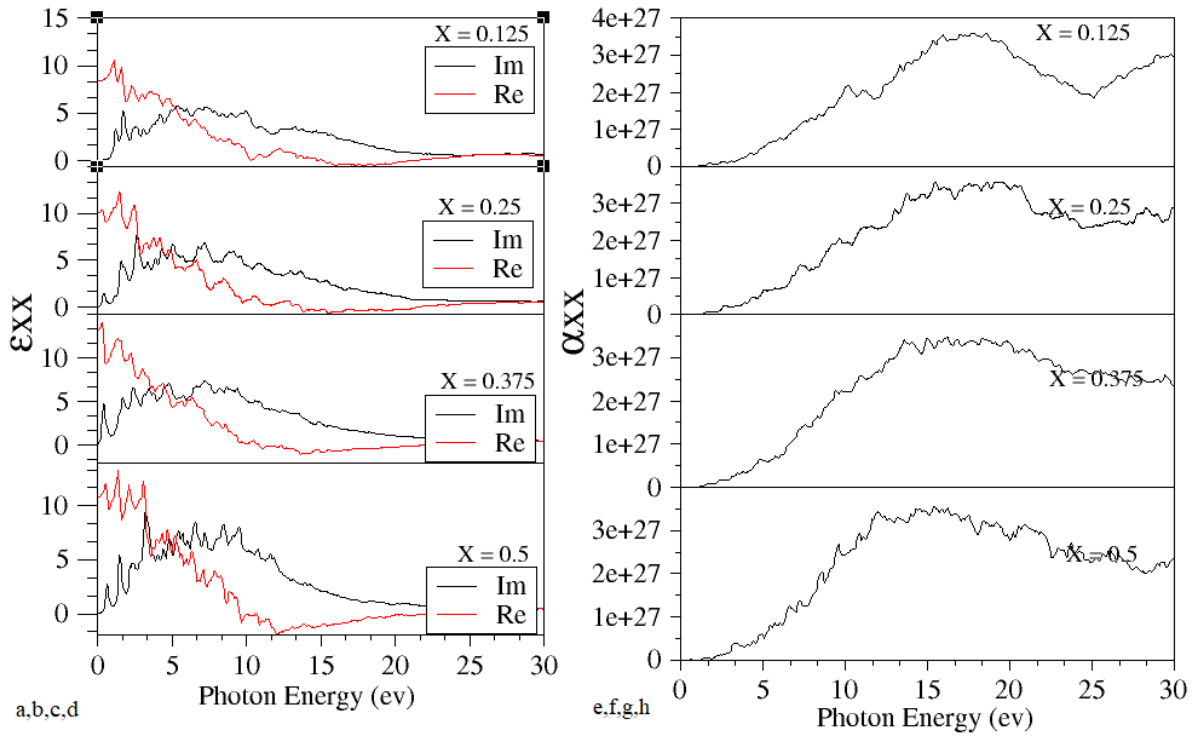


Figure 8: Real and imaginary part of the dielectric function of the doped  $\text{CoO}_{1-x}\text{S}_x$  at doping concentration, (a)  $x = 0.125$  (b)  $x = 0.25$  (c)  $x = 0.375$  (d)  $x = 0.5$  (left panel). Absorption coefficient spectrum of  $\text{CoO}_{1-x}\text{S}_x$  at (e)  $x = 0.125$  (f)  $x = 0.25$  (g)  $x = 0.375$  (h)  $x = 0.5$  (right panel)

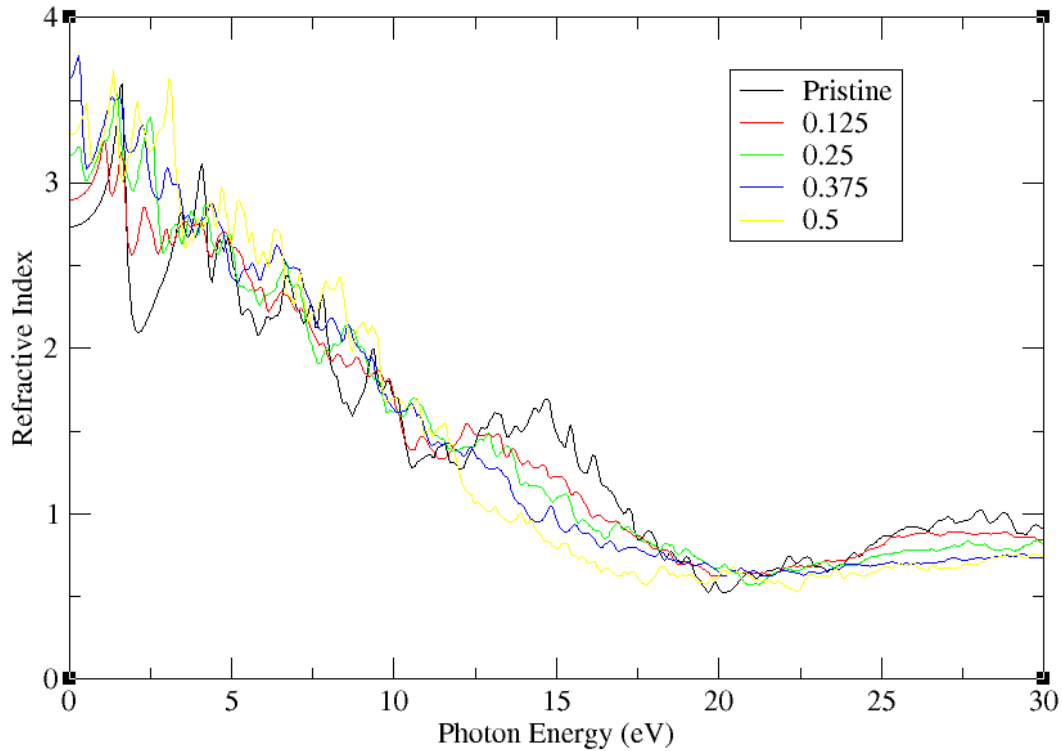


Figure 9. The refractive index of  $\text{CoO}_{1-x}\text{S}_x$  at sulphur doping concentration,  $x = 0.125, 0.25, 0.375,$  and  $0.5$ .

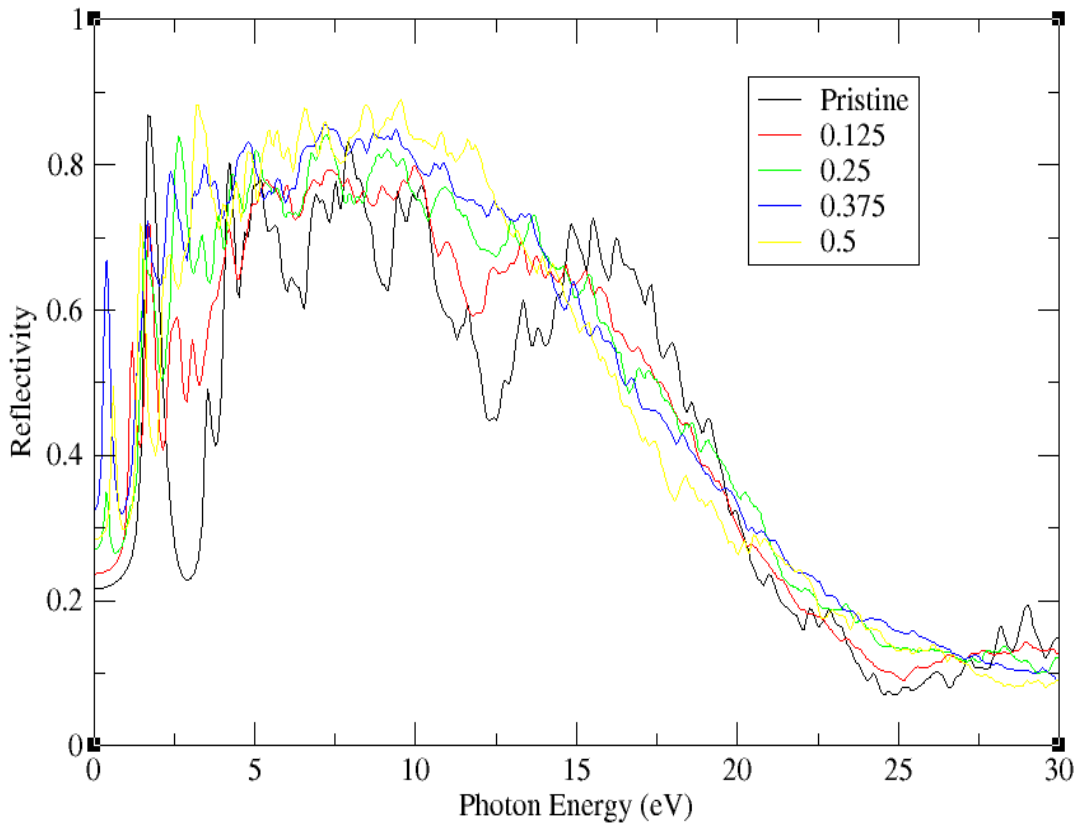


Figure 10. The reflectivity index of pristine CoO and CoO<sub>1-x</sub>S<sub>x</sub> at doping concentration  $x = 0.125, 0.25, 0.375,$  and  $0.5$ .

### 3.4 Magnetic properties

We have presented the magnetic moment of the pristine CoO and sulphur doped CoO at sulphur concentrations of 0.125, 0.25, 0.375, and 0.5, for both GGA and GGA+U in Table 2.

Table 2: Magnetic moments of sulphur doped CoO at 0.125, 0.25, 0.375, and 0.5 for GGA and GGA+U calculations.  $M_{Co}$ ,  $M_O$ ,  $M_S$  and  $M_T$  are the magnetic moment on Co atom, O atom, S atom and total magnetic moment per formula unit of the pristine or doped CoO compound respectively at various doping concentration  $x$ .

x	$M_{Co}$ ( $\mu_B$ )		$M_O$ ( $\mu_B$ )		$M_S$ ( $\mu_B$ )		$M_T$ ( $\mu_B$ )	
	GGA	GGA+U	GGA	GGA+U	GGA	GGA+U	GGA	GGA+U
0	2.2294	2.3436	0.1996	0.1967	-	-	2.4290	2.5403
0.125	2.0409	2.5722	0.1592	0.1851	-0.0543	-0.1187	2.1458	2.6386
0.25	2.0960	2.6273	0.2143	0.2236	0.0008	0.1814	2.2009	3.0323
0.375	0.1615	2.4449	-0.2357	0.1304	0.0022	0.1801	-0.0720	2.7554
0.5	1.0333	2.6290	0.1107	0.1954	0.0226	0.1567	1.1666	2.9811

Antiferromagnetic ground state was obtained for the pristine and doped CoO compounds. For ordinary GGA, the pure CoO's total magnetic moment per formula unit ( $M_T$ ) is initially high at 2.4290  $\mu_B$  but drops as the sulphur doping concentration rises. However, the total magnetic moment at the doping concentration of 0.25 is higher than that of 0.125. This further emphasizes that there is a strong hybridization between the Co, O and S atoms at  $x = 0.25$  suggesting that this

might be the optimal sulphur doping concentration for the cubic CoO. Sulphur doping simply weakens the magnetic ordering in the CoO system because the local magnetic moment on the sulphur atoms is lower than that on the oxygen atoms. However, for GGA+U computations, the doped CoO's total magnetic moment per formula unit ( $M_T$ ) is greater than the pure CoO's and rises with the doping concentration of sulfur. Like the GGA result, the magnetic moment at the doping concentration at  $x = 0.25$  distorts the increasing order of the magnetic moment with doping concentration. Notably, the local magnetic moment of sulphur ( $M_S$ ) at doping concentrations of 0.125 and 0.375 are negative showing that they are antialigned to the local magnetic moment of cobalt and oxygen. Magnetic moments per formula unit calculated using GGA+U are generally higher than that obtained using standard. This can be attributed to the inclusion of the Hubbard U correction, which accounts for the on-site Coulomb repulsion of electrons, thereby enhancing the magnetic moments.

#### 4. Conclusion

We have examined the structural, electronic, optical, and magnetic characteristics of the pristine and doped cubic CoO compound using first principles DFT. According to our findings, one of the main benefits of doping CoO with sulfur is the reduction of the energy band gap, which improves solar absorption in the visible range for effective photovoltaic and other applications. We used Hubbard U parameter of 5.7347 eV, which was calculated using the self-consistent linear response approach developed by Cococcioni and his group for GGA+U computations. Our result shows that GGA+U gives more accurate electronic and optical properties of the compounds studied than the GGA when compared with the experimental results. Overall, our findings contribute to the fundamental understanding of the effects of non-metal doping on CoO transition metal oxide and paves way for its utilization in various technological applications, including solar energy conversion, energy storage, photo-catalysis, and other applications.

#### Acknowledgement

The computational facility are provided by the Lehigh HPC, United States and Center for High Performance Computing (CHPC), South Africa under MATS0988. ATR, affirms that this research work forms part of the research project supported by the National Research Foundation (NRF, South Africa; <https://www.nrf.ac.za/>) with Project Grant Number: 141942."

#### Reference

- [1] U. D. Wdowik and K. Parlinski, "Lattice dynamics of CoO from first principles," *Phys Rev B Condens Matter Mater Phys*, vol. 75, no. 10, Mar. 2007, doi: 10.1103/PhysRevB.75.104306.
- [2] S. O. Aisida *et al.*, "Microstructural and magneto-optical properties of Co<sub>1-x</sub>Ni<sub>x</sub> Fe<sub>2</sub>O<sub>4</sub> nanocomposites for hyperthermia applications," *Solid State Sci*, vol. 136, Feb. 2023, doi: 10.1016/j.solidstatesciences.2022.107107.
- [3] K. O. Egbo, T. C. Chibueze, A. T. Raji, C. E. Ekuma, C. P. Liu, and K. M. Yu, "Effects of acceptor doping and oxygen stoichiometry on the properties of sputter-deposited p-type rocksalt Ni<sub>x</sub>Zn<sub>1-x</sub>O (0.3 ≤ x ≤ 1.0) alloys," *J Alloys Compd*, vol. 905, Jun. 2022, doi: 10.1016/j.jallcom.2022.164224.
- [4] T. C. Chibueze and C. M. I. Okoye, "First principles study of the structural, electronic and magnetic properties of w-CoS," *Physica B Condens Matter*, vol. 554, pp. 165–172, Feb. 2019, doi: 10.1016/j.physb.2018.11.019.

- [5] C. Zheng, C. Cao, Z. Ali, and J. Hou, "Enhanced electrochemical performance of ball milled CoO for supercapacitor applications," *J Mater Chem A Mater*, vol. 2, no. 39, pp. 16467–16473, Oct. 2014, doi: 10.1039/c4ta02885f.
- [6] Q. Zhang, Z. Jin, F. Li, Z. Xia, Y. Yang, and L. Xu, "First application of CoO nanorods as efficient counter electrode for quantum dots-sensitized solar cells," *Solar Energy Materials and Solar Cells*, vol. 206, Mar. 2020, doi: 10.1016/j.solmat.2019.110307.
- [7] W. S. Seo, J. H. Shim, S. J. Oh, E. K. Lee, N. H. Hur, and J. T. Park, "Phase- and size-controlled synthesis of hexagonal and cubic CoO nanocrystals," *J Am Chem Soc*, vol. 127, no. 17, pp. 6188–6189, May 2005, doi: 10.1021/ja050359t.
- [8] S. Grytsyuk and U. Schwingenschlögl, "Mechanism of magnetization enhancement at CoO/permalloy interfaces," *Appl Phys Lett*, vol. 103, no. 7, Aug. 2013, doi: 10.1063/1.4818507.
- [9] U. D. Wdowik and K. Parlinski, "Electronic structure of cation-deficient CoO from first principles," *Phys Rev B Condens Matter Mater Phys*, vol. 77, no. 11, Mar. 2008, doi: 10.1103/PhysRevB.77.115110.
- [10] S. N. F. Moridon, K. Arifin, A. Linggawati, L. J. Minggu, and M. Bin Kassim, "Density Functional Theory Study on the Electronic Properties of Doped-Cobalt Oxide (CoO)," *Jurnal Kejuruteraan*, vol. 32, no. 1, pp. 61–66, Feb. 2020, doi: 10.17576/jkukm-2020-32(1)-08.
- [11] B. Zhou, X. Zhao, H. Liu, J. Qu, and C. P. Huang, "Visible-light sensitive cobalt-doped BiVO<sub>4</sub> (Co-BiVO<sub>4</sub>) photocatalytic composites for the degradation of methylene blue dye in dilute aqueous solutions," *Appl Catal B*, vol. 99, no. 1–2, pp. 214–221, Aug. 2010, doi: 10.1016/j.apcatb.2010.06.022.
- [12] S. Grytsyuk and U. Schwingenschlögl, "Mechanism of magnetization enhancement at CoO/permalloy interfaces," *Appl Phys Lett*, vol. 103, no. 7, Aug. 2013, doi: 10.1063/1.4818507.
- [13] X. Feng *et al.*, "Converting ceria polyhedral nanoparticles into single-crystal nanospheres," *Science (1979)*, vol. 312, no. 5779, pp. 1504–1508, Jun. 2006, doi: 10.1126/science.1125767.
- [14] M. Y. Yin, X. C. Wang, W. B. Mi, Y. H. Ding, G. F. Chen, and B. H. Yang, "Magnetism and electronic structure in Zn and Ti doped CoO: A first-principles study," *Comput Mater Sci*, vol. 93, pp. 193–200, 2014, doi: 10.1016/j.commatsci.2014.06.016.
- [15] R. X. Liu, X. C. Wang, G. F. Chen, and B. H. Yang, "Magnetism and electronic structure in La-doped CoO: A first-principles study," *Physica E Low Dimens Syst Nanostruct*, vol. 74, pp. 226–232, Jul. 2015, doi: 10.1016/j.physe.2015.07.008.
- [16] R. X. Liu, X. C. Wang, G. F. Chen, and B. H. Yang, "First-principles study on the magnetism and electronic structure in 3d transition metal (X=Sc, V, Cr, Mn, Fe, Ni, Cu) doped CoO," *Physica E Low Dimens Syst Nanostruct*, vol. 77, pp. 149–155, Mar. 2016, doi: 10.1016/j.physe.2015.11.022.
- [17] C. Chen *et al.*, "Controllable synthesis of Cu-doped CoO hierarchical structure for high performance lithium-ion battery," *J Power Sources*, vol. 314, pp. 66–75, May 2016, doi: 10.1016/j.jpowsour.2016.02.085.

- [18] Y. J. Li *et al.*, “Multiscale Structural Engineering of Ni-Doped CoO Nanosheets for Zinc–Air Batteries with High Power Density,” *Advanced Materials*, vol. 30, no. 46, Nov. 2018, doi: 10.1002/adma.201804653.
- [19] A. Van De Walle, M. Asta, and G. Cederb, “The Alloy Theoretic Automated Toolkit: A User Guide,” 2002.
- [20] I. E. Gaa, P. Hohenberg, E. Artacho, X. Sun, F. And, and W. Konnt, “PHYSICAL REVIEW.”
- [21] W. Kohn and L. J. Sham, “PHYSICAL REVIEW Self-Consistent Equations Including Exchange and Correlation Effects\*.”
- [22] P. Giannozzi *et al.*, “QUANTUM ESPRESSO: A modular and open-source software project for quantum simulations of materials,” *Journal of Physics Condensed Matter*, vol. 21, no. 39, 2009, doi: 10.1088/0953-8984/21/39/395502.
- [23] “physrevlett.43.1494 j”.
- [24] H. J. Monkhorst, “Hartree-Fock density of states for extended systems.”
- [25] S. Rodríguez, C. Zandalazini, J. Navarro, K. T. Vadiraj, and E. A. Albanesi, “First principles calculations and experimental study of the optical properties of Ni-doped ZnS,” *Mater Res Express*, vol. 7, no. 1, 2019, doi: 10.1088/2053-1591/ab5cd2.
- [26] S. L. Dudarev, G. A. Botton, S. Y. Savrasov, C. J. Humphreys, and A. P. Sutton, “Electron-energy-loss spectra and the structural stability of nickel oxide: An LSDAU study,” 1998.
- [27] I. Timrov, N. Marzari, and M. Cococcioni, “Hubbard parameters from density-functional perturbation theory,” *Phys Rev B*, vol. 98, no. 8, Aug. 2018, doi: 10.1103/PhysRevB.98.085127.
- [28] I. Timrov, N. Marzari, and M. Cococcioni, “Self-consistent Hubbard parameters from density-functional perturbation theory in the ultrasoft and projector-augmented wave formulations,” *Phys Rev B*, vol. 103, no. 4, Jan. 2021, doi: 10.1103/PhysRevB.103.045141.
- [29] F. Tran, P. Blaha, K. Schwarz, and P. Novák, “Hybrid exchange–correlation energy functionals for strongly correlated electrons: Applications to transition-metal monoxides,” *Phys Rev B Condens Matter Mater Phys*, vol. 74, no. 15, 2006, doi: 10.1103/PhysRevB.74.155108.
- [30] G. Fischer *et al.*, “Exchange coupling in transition metal monoxides: Electronic structure calculations,” *Phys Rev B Condens Matter Mater Phys*, vol. 80, no. 1, Aug. 2009, doi: 10.1103/PhysRevB.80.014408.
- [31] E. Z. Kurmaev, R. G. Wilks, A. Moewes, L. D. Finkelstein, S. N. Shamin, and J. Kuneš, “Oxygen x-ray emission and absorption spectra as a probe of the electronic structure of strongly correlated oxides,” *Phys Rev B Condens Matter Mater Phys*, vol. 77, no. 16, Apr. 2008, doi: 10.1103/PhysRevB.77.165127.
- [32] P. De, V. Du Plessis, S. J. Van Tonder, and L. Alberts, “Elastic constants of a NiO single crystal: I (Magnetic transitions) Elastic constants of a NiO single crystal: It,” 1971. [Online]. Available: <http://iopscience.iop.org/0022-3719/4/14/013>

- [33] N. Tuan Hung, A. R. T Nugraha, and R. Saito, “Quantum ESPRESSO Course for Solid-State Physics.indd.”
- [34] A. Taya, P. Rani, J. Thakur, and M. K. Kashyap, “First principles study of structural, electronic and optical properties of Cs-doped CH<sub>3</sub>NH<sub>3</sub>PbI<sub>3</sub> for photovoltaic applications,” *Vacuum*, vol. 160, pp. 440–444, Feb. 2019, doi: 10.1016/j.vacuum.2018.12.008.
- [35] M. Khuili, N. Fazouan, H. Abou El Makarim, E. H. Atmani, D. P. Rai, and M. Houmad, “First-principles calculations of rare earth (RE=Tm, Yb, Ce) doped ZnO: Structural, optoelectronic, magnetic, and electrical properties,” *Vacuum*, vol. 181, Nov. 2020, doi: 10.1016/j.vacuum.2020.109603.